ITERATIVE MULTIFRAME SUPER-RESOLUTION ALGORITHMS FOR ATMOSPHERIC TURBULENCE-DEGRADED IMAGERY

David G. Sheppard, Bobby R. Hunt, Michael W. Marcellin

Department of Electrical and Computer Engineering
University of Arizona
Tucson, AZ 85721

ABSTRACT

Algorithms for image recovery with super-resolution from sequences of short-exposure images are presented in this paper. Both deconvolution from wavefront sensing (DWFS) and blind deconvolution are explored. A multiframe algorithm is presented for DWFS which is based on maximum a posteriori (MAP) formulation. A multiframe blind deconvolution algorithm is presented based on a maximum likelihood formulation with strict constraints incorporated using nonlinear reparameterizations. Quantitative simulation of imaging through atmospheric turbulence and wavefront sensing are used to demonstrate the super-resolution performance of the algorithms.

1. INTRODUCTION

The study of space objects (SO) such as satellites is growing in importance. Most, if not all, SO images are acquired by ground-based optical systems observing through the turbulent earth atmosphere. Turbulence-induced inhomogeneities in the atmosphere cause severe degradation of the images and are the chief obstacle to obtaining high resolution SO images with large aperture telescopes. The area of interest in this paper is restoration of SO imagery with *super-resolution.* Super-resolution may be defined formally as the removal of blur caused by a diffraction-limited optical system along with meaningful recovery of object spatial frequency components outside the optical system passband [1, 10, 4]. This definition is adequate for the current context, in which the combined atmosphere/telescope optical transfer function (OTF) replaces the diffraction-limited OTF.

The super-resolution algorithms presented below for SO images are based on processing sequences of short exposure images, or frames, in deconvolution from wave front sensing (DWFS) [8] and blind deconvolution modes. Using multiple frames has advantages both in terms of image information content [7] and noise control. Averaging the frames (approximating the long-exposure image) is less effective because the object spatial frequency content in each of the frames is severely attenuated [7]. In the DWFS case, wave front sensor measurements are taken for each frame and used to estimate the optical transfer function (OTF). A multiframe maximum a posteriori algorithm [3, 6] is presented for this task. In the blind deconvolution case, the OTF for each frame is unknown and must be recovered during the deconvolution process. The key to making blind methods work is the application of *a priori* knowledge about the nature of the degradations and the images, and using multiple differently blurred frames is in itself a powerful constraint on the restored original object image. The algorithms presented below extend the work of Conan and Thiébaut [12] to the multiframe problem and are based on Bayes maximum likelihood criteria for Poisson data.

2. ITERATIVE MULTIFRAME SUPER-RESOLUTION ALGORITHMS

In this section, iterative multiframe algorithms are derived for both deconvolution from wave front sensing and blind deconvolution.

2.1. Multiframe Poisson MAP Algorithms for Deconvolution from Wave Front Sensing

Given an object image f, let $\{g_k\}_{k=1}^{K}$ and $\{h_k\}_{k=1}^{K}$ be a sequence of observed images and the sequence of atmosphere/telescope point spread functions (PSF) which correspond to them. Discrete-to-discrete image formation [1] is assumed with the object plane indexed by coordinates i and j, and the image plane indexed by coordinates x and y. Bayes rule provides a complete description of the conditional probabilistic relationship between the object, f, and the sequence of recorded images:

$$p\left(f, \{h_k\} \mid \{g_k\}\right) = \frac{p\left(\{g_k\} \mid f, \{h_k\}\right) p\left(f, \{h_k\}\right)}{p\left(\{g_k\}\right)}. \qquad (1)$$

In the following development, it is assumed that PSF estimates have been produced from WFS measurements. They will not be treated as statistical quantities as is possible in general. Assuming that the observed images are statistically independent,[1] the maximum a posteriori (MAP) estimate is given by

$$\begin{aligned} \hat{f} &= \arg\max_f \, p\left(\{g_k\} \mid f\right) p\left(f\right) \\ &= \arg\max_f \, p\left(f\right) \prod_k p\left(g_k \mid f\right) \qquad (2) \\ &= \arg\max_f \, \sum_k \ln p(g_k \mid f) + \ln p_f(f) \qquad (3) \end{aligned}$$

after taking the natural logarithm of the right hand side of Equation (2). Solution of Equation (3) can be obtained by noting that it is sufficient to solve the system of equations

$$\sum_k \frac{\partial}{\partial f_{ij}} \left[\ln p(g_k \mid f)\right]\Big|_{\hat{f}} + \frac{\partial}{\partial f_{ij}} \left[\ln p(f)\right]\Big|_{\hat{f}} = 0, \qquad (4)$$

[1] It is important to note that the assumptions about statistical independence are acknowledged to be generally incorrect. They are made solely for the purpose of mathematical tractability.

By assuming Poisson emission and observation models for the object and image, respectively, the multiframe Poisson MAP algorithm is given by

$$f_{ij}^{n+1} = \bar{f}_{ij}^{n} \prod_{k} \exp\left\{ \frac{1}{K} \left[\left(\frac{g_k}{(f^n * h_k)} - 1 \right) * h_k^+ \right]_{ij} \right\}, \quad (5)$$

where K is the number of data frames, and the notation h_k^+ refers to the adjoint of h_k $\left(\left(h_k^+\right)_{i,j} = \left(h_k\right)^*_{-i,-j} \right)$. The object mean emission rate $\bar{f}_{ij}$ is generally unknown and implementation of Equation (5) is not possible without some additional knowledge about the object. This term can be useful for incorporating models for the object in the form of Markov random fields [11]. In the absence of such a model, one may adopt the heuristic approach that the latest estimate embodies the best knowledge about the object prior distribution. Making the substitution $\bar{f}_{ij} = f_{ij}$ yields the baseline multiframe Poisson MAP algorithm. The computational requirements of this algorithm increase linearly with the number of frames. A more efficient algorithm, referred to as the incremental version, may be derived by using the single frame PMAP algorithm with a different pair $\{g_k, h_k\}$ at each iteration. These pairs may be drawn at random from the data set or in sequence. It has the same computational requirements as the single frame version while offering nearly identical super-resolution performance.

2.2. A Multiframe Maximum Likelihood Blind Deconvolution Algorithm with Strict Constraints

The multiframe maximum likelihood estimate can be reformulated as a minimization problem

$$\hat{f} = \arg\min_{f,\{h_k\}} \left[-\ln p\left(\{g_k\} \middle| f \right) \right] \quad (6)$$

where the PSF values are treated as free parameters in the above model. A distributional assumption about them is not made. Poisson statistics are assumed for the observed image. Making the distributional substitution in Equation (6) yields the objective function, denoted by $J(f)$,

$$\begin{aligned} J(f) &= -\sum_k \sum_{x,y} \ln p\left((g_k)_{xy} \middle| f \right) \\ &\approx -\sum_k \sum_{x,y} (g_k)_{xy} \ln\left[(f * h_k)_{xy} \right] \\ &\quad - (f * h_k)_{xy} \end{aligned} \quad (7)$$

An expression for the gradient with respect to f_{ij} is given by

$$\frac{\partial J(f)}{\partial f_{ij}} = -\sum_k \left[\left(\frac{g_k}{(f * h_k)} - 1 \right) * h_k^+ \right]_{ij}. \quad (8)$$

Strict positivity is imposed on f_{ij} by reparameterizing it as $f_{ij} = \varphi_{ij}^2$, where φ_{ij} is free to take on any value. Enforcing constraints in this manner was proposed by Biraud [2] and revived for blind deconvolution of astronomical images by Conan and Thiébaut [12]. The components of the gradient can be found in terms of the φ_{ij} by applying the chain rule to yield

$$\begin{aligned} \frac{\partial J(f)}{\partial \varphi_{ij}} &= \frac{\partial J(f)}{\partial f_{ij}} \frac{\partial f_{ij}}{\partial \varphi_{ij}} \\ &= -2\varphi_{ij} \sum_k \left[\left(\frac{g_k}{(f * h_k)} - 1 \right) * h_k^+ \right]_{ij}. \end{aligned} \quad (9)$$

At this point, it is necessary to compute the components of the objective function gradient with respect to the PSF parameters. A three-fold reparameterization of the point spread function enforces positivity, unit volume, and finite bandwidth simultaneously. This is given by

$$(h_k)_{ij} = \frac{(\xi * \psi_k)_{ij}^2}{\sum\limits_{i',j'} (\xi * \psi_k)_{i'j'}^2} \quad (10)$$

where the ψ_k are the free parameters and ξ is a low pass filter kernel designed to imposed a finite bandwidth on the PSF. The cutoff frequency of ξ should be set to half the optical cutoff frequency of the optical system because squaring the result of $\xi * \psi_k$ results in a doubling of the bandwidth. The gradient in terms of the ψ_k parameters can be found using the chain rule, as shown in Equation (11), where the dummy coordinates m and n index the object plane. With closed form expressions for the objective function and its gradients, the problem may be solved with any number of gradient descent-type methods. The method of conjugate gradients was used to solve this problem.

3. SIMULATION RESULTS

The HYSIM3 simulation software developed at the Air Force Institute of Technology was used to simulate short-exposure image formation through atmospheric turbulence. It was also used to simulate Shack-Hartmann WFS performance. The parameters of the simulation are intended to model image acquisition using a 1.6 m telescope with a central obscuration of 0.335 m. Each wave front sensor subaperture corresponds to a 10 cm telescope subaperture. Due to space limitations, results from only one case will be shown: that of a visual magnitude four satellite viewed through an atmosphere with a Fried parameter of 10 cm. Many other values of these parameters were studied, and the algorithms performed predictably. Figure 1 shows the original OCNR5 satellite object image and a short-exposure image generated using the HYSIM3 code, and corresponding Fourier spectra. All images are 256×256 in size. The optical cutoff of the instrument is located at half the folding frequency. Because the data is oversampled, no upsampling is carried out. In many practical situations, the recorded images are Nyquist-sampled or even under-sampled. In such cases, it is necessary to upsample the restorations in order to avoid aliasing caused by the super-resolution of the restored image [3].

3.1. Multiframe Poisson MAP Results

Two versions of the multiframe PMAP algorithm were presented above: the baseline and incremental versions. From testing both of these algorithms, it was found that the results produced by the two were nearly identical in all cases. This is striking because the computational requirements are quite different. Many cases were considered and the near equivalence was uniform throughout. The results presented in this section for the PMAP algorithm were produced by the incremental version. Figure 2 show the Poisson MAP algorithm restorations from uncompensated images for varying numbers of frames. The algorithms were allowed to run for 1000 iterations. In many cases, this corresponds to early termination of the algorithm's progress. Clearly, using more frames produces better restorations. Super-resolution is evident in the restored spectra. For fainter objects, more frames are required to maintain the quality of the restoration. Restorations from $m_v = 8$

$$
\begin{aligned}
\frac{\partial J\left(f,\{h_k\}\right)}{\partial\left(\psi_k\right)_{ij}} &= \sum_{m,n}\frac{\partial J\left(f,\{h_k\}\right)}{\partial\left(h_k\right)_{mn}}\frac{\partial\left(h_k\right)_{mn}}{\partial\left(\psi_k\right)_{ij}} \\
&= -\left(\frac{2}{\sum\limits_{i',j'}\left(\xi*\psi_k\right)^2_{i'j'}}\right)\left[\left[\left(\left(\xi*\psi_k\right)\left(\frac{g_k}{f*h_k}-1\right)*f^+\right)*\xi^+\right]_{ij}\right. \\
&\qquad \left. -\left[\left(\xi*\psi_k\right)*\xi^+\right]_{ij}\sum_{m,n}\left[\left(\frac{g_k}{f*h_k}-1\right)*f^+\right]_{mn}\left(h_k\right)_{mn}\right] \qquad (11)
\end{aligned}
$$

data demonstrate that the algorithms are near the lower limits of acceptable performance and that 200 frames are required to obtain a reasonable restoration. Both the SNR of the data and the worsening performance of the WFS system are contributing factors in the decline of performance with decreasing object brightness.

3.2. Multiframe Blind Deconvolution Results

Figure 3 shows blind deconvolution results produced from the same data used to test the PMAP algorithm. As expected, the results from the blind algorithm are not as good as the DWFS results in which the OTF for each frame is measured. The results are encouraging, however. Super-resolution is in evidence, although not to the same degree. The algorithm was implemented in C code on the parallel IBM SP2 using the Message Passing Interface (MPI) in order to make the execution time manageable.

4. CONCLUSION

New multiframe algorithms for constrained nonlinear deconvolution from wave front sensing and blind deconvolution were presented. Additionally, super-resolution of extended space object images was demonstrated in both the DWFS and blind cases using careful simulation of imaging through atmospheric turbulence. The use of multiple frames in the design of the algorithms was instrumental in controlling the noise present in photon-limited images without suppressing object spectral content in the individual frames, and for regularizing the blind deconvolution process. The results indicate that post-processing of uncompensated images may be a viable alternative to building fully compensated adaptive optics systems. Retrofitting existing large telescopes with wave front sensor systems may also be the most effective way of bringing them into the modern era of image recovery. It should be stressed that when real time image recovery is critical, the approaches presented above do not provide a viable alternative to adaptive optics. The results produced by blind deconvolution were not quite as good as those from wave front sensing, which is not surprising given the inherent difficulty of the problem. However, they demonstrate that good image recovery is possible in this mode of operation for extended satellite objects.

Acknowledgments

The authors wish to express their appreciation to Dr. Michael Roggeman for providing the HYSIM3 software and for helpful advice regarding wave front sensing simulation. This research was supported by the U.S. Air Force under contract number SC-92C-04-31.

5. REFERENCES

[1] H. C. Andrews and B. R. Hunt, *Digital Image Restoration* (Prentice-Hall: Englewood Cliffs, NJ), 1977.

[2] Y. Biraud, "A new approach for increasing the resolving power by data processing," *Astron. & Astrophys.*, vol. 1, no. 1, Jan. 1969, 124-7.

[3] B. R. Hunt and P. J. Sementilli, "Description of a Poisson imagery super-resolution algorithm," in *Astronomical Data Analysis Software and Systems I*, D. Worral, C. Biemesderfer and J. Barnes, eds. (Astronomy Society of the Pacific: San Francisco), 1992, 196-99.

[4] B. R. Hunt, "Super-resolution of images: algorithms, principles, performance," *Int. J. Imaging Sys. and Tech.*, vol. 6, winter 1995, 297–304.

[5] S. M. Jefferies and J. C. Christou, "Restoration of astronomical images by iterative blind deconvolution," *Astrophys. J.*, vol. 415, no. 2, 1 Oct. 1993, 862-74.

[6] E. S. Meinel, "Origins of linear and nonlinear recursive restoration algorithms," *J. Opt. Soc. Am. A*, vol. 3, no. 6, June 1986, 787-99.

[7] F. Roddier, "The effects of atmospheric turbulence in optical astronomy," in *Progress in Optics XIX*, E. Wolf, ed. (North-Holland, Amsterdam, Netherlands), 1981, 281-376.

[8] M. C. Roggeman and B. Welsh, *Imaging Through Turbulence* (CRC Press: New York, NY), 1996.

[9] T. J. Schulz, "Multiframe blind deconvolution of astronomical images," *J. Opt. Soc. Am. A*, vol. 10, no. 5, May 1993, 1064-73.

[10] P. J. Sementilli, B. R. Hunt, and M. S. Nadar, "Analysis of the limit to super-resolution in incoherent imaging," *J. Opt. Soc. Am. A*, vol. 10, no. 11, Nov. 1993, 2265–76.

[11] P. J. Sementilli, "Suppression of artifacts in super-resolved images," Ph.D. Dissertation, University of Arizona, Tucson 1993.

[12] E. Thiébaut and J.-M Conan, "Strict a priori constraints for maximum-likelihood blind deconvolution," *J. Opt. Soc. Am. A*, vol. 12, no. 3, Mar. 1995, 485-92.

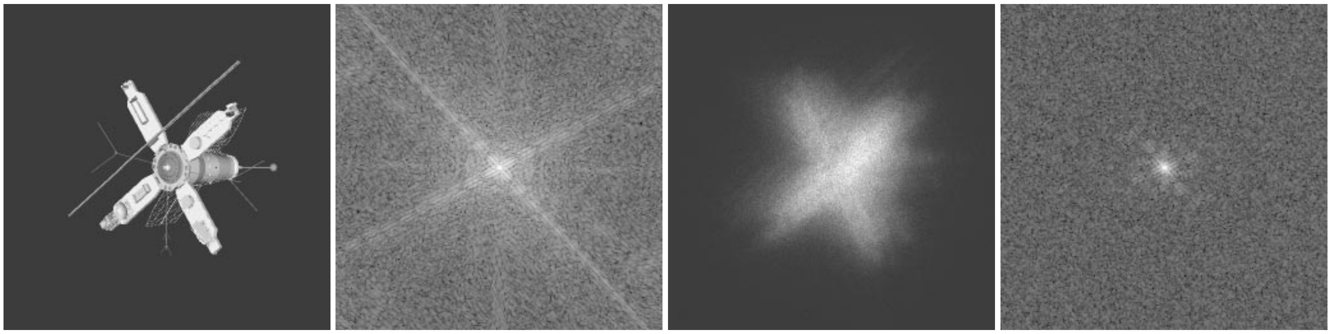

(a) OCNR5 object (b) OCNR5 object spectrum (c) $m_v = 4$ frame (d) $m_v = 4$ frame spectrum

Figure 1: Computer rendered OCNR5 satellite object and a simulated short-exposure image at visual magnitude $m_v = 4$ ($r_0 = 10$ cm), and associated spectra. All spectra are range compressed using $\log_{10}(1 + |\cdot|^2)$.

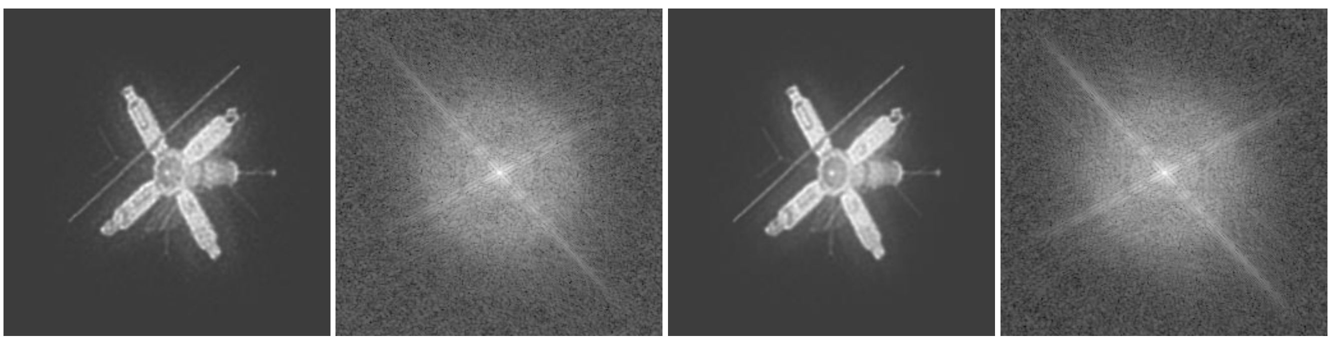

(a) 50 frame restoration (b) 50 frame restored spectrum (c) 200 frame restoration (d) 200 frame restored spectrum

Figure 2: Restoration of visual magnitude $m_v = 4$ OCNR5 object using the multiframe incremental Poisson MAP algorithm with varying number of frames ($r_0 = 10$ cm), and associated spectra. All spectra are range compressed using $\log_{10}(1 + |\cdot|^2)$.

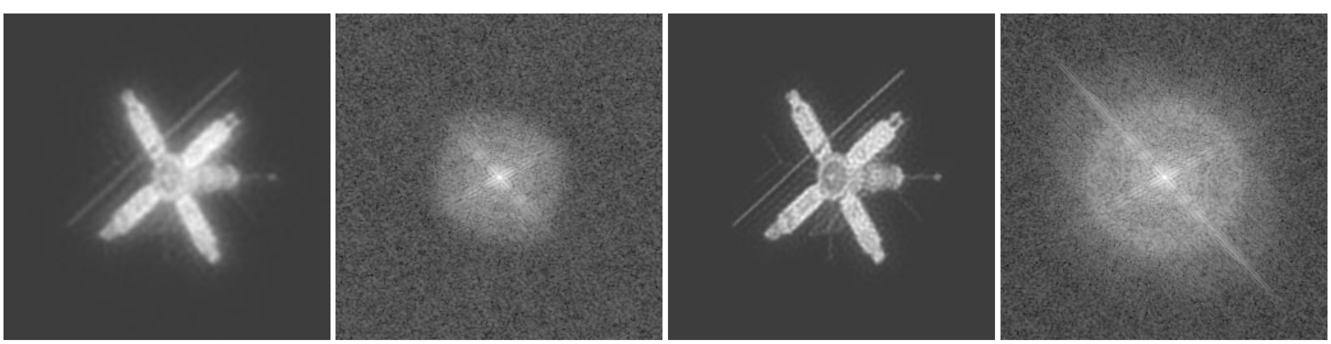

Figure 3: Restoration of visual magnitude $m_v = 4$ OCNR5 object using the multiframe maximum likelihood blind deconvolution algorithm with varying number of frames ($r_0 = 10$ cm), and associated spectra. All spectra are range compressed using $\log_{10}(1 + |\cdot|^2)$.